JOURNAL OF COMPUTATIONAL PHYSICS **132,** 215–225 (1997)
ARTICLE NO. CP965586

High Resolution Computations of Ocean Wave Spectral Modulations due to Two-Dimensional Wave–Current Interactions

R. A. Fusina, A. L. Cooper, and S. R. Chubb

Remote Sensing Division, Naval Research Laboratory, Code 7253, Washington, DC 20375-5351

Received August 9, 1995; revised September 11, 1996

A new nesting technique has been developed for computing solutions of the steady-state form of the wave action equation. The technique is especially useful for investigating the effects of resolution on the accuracy and stability of the computation. This has importance in the problem of determining ocean wave spectra under the influence of ambient wind fields and current distributions. The technique enables extremely high resolution computations to be performed with minimal computer storage requirements. It is especially useful for applications in modelling radar imagery of the ocean surface. Investigations of the convergence, stability, and accuracy of the procedure are made possible by introducing a fixed grid point location which is common to all the nested grids. In order to display the method, we apply it to a particular model of an oceanographic current rip feature that was recently observed during the first High Resolution Remote Sensing Experiment. Limitations of the method are also discussed.

I. INTRODUCTION

The wave action equation characterizes the effects of winds and currents upon the ocean wave spectrum. It is an expression of conservation of wave action spectral density with the inclusion of source terms to simulate the real world effects of wind wave growth, dissipation, and nonlinear wave–wave interactions. Although the solution of the wave action equation is traditionally an initial value problem, there exists a particular steady-state limit of the equation where the solution can be transformed into a boundary value problem. When applied to problems encompassing large spatial extent, this limit can be conveniently used for determining the spectrum of waves at the surface of the ocean, when a particular form of source function is used. In order to simulate the radar imagery of oceanographic features, it is necessary to determine the associated variation in the corresponding ocean wave spectra. To accomplish this, a number of questions must be addressed, related to spatial and spectral resolution, convergence, and the uniqueness of the solution. Even in the steady-state limit, the differential equation involves four explicit variables. For the solution to be meaningful, it must approach a unique solution. The resolution (both spatial and spectral) must be sufficiently fine to ensure that the solution will be insensitive to more finely resolved variations in scale. Ensuring uniqueness can be a formidable task because of variability of the four-dimensional space associated with the problem. A second, potentially more fundamental requirement is to identify a suitable choice of appropriate boundary conditions which can be related to the known dynamics of the equation, relative to the surface feature under consideration.

In the present paper, we demonstrate the utility of a nesting technique for constructing solutions that satisfy these last two criteria. In particular, in the technique, wave-action spectral densities associated with the solution of the equation from one spatial grid are used to provide updated boundary conditions for calculations that are performed on a smaller, embedded grid. This process is repeated until the desired resolution for a region of interest is obtained. We have tested the technique and demonstrated its utility using a particular model of an oceanographic feature that was observed during a recent experiment. An unexpected result is that, provided the numerical grid that is selected possesses adequate spectral resolution, it is possible to obtain a well-converged solution of the wave action equation, on a scale that is significantly more finely resolved spatially, with a minimal number of applications of the nesting procedure.

Previously, a nesting approach has been developed for determining wave spectra based on embedded spatial grids [1]. However, this earlier method, which is applicable for the time-dependent WAM model, is more useful for larger scale problems involving mesoscale spatial extent, where the WAM model has been applied. The approach is also inherently more computationally intensive because it is based on solving the time-dependent, nonsteady-state problem. The method presented in this paper is inherently faster because it is based on the boundary value problem that can be applied to uses involving the simpler, steady-state approximation. Also, the present method can be more readily applied to the problems associated with considerably smaller spatial extent.

The paper is organized as follows. In Part II, we describe the wave action equation and the full-wave method for its

0021-9991/97 $25.00

solution. Part III describes the new nesting technique. Part IV details the experimental results and our modeling effort, and the results of our calculations are reported in part V. Part VI is a summary.

II. THE WAVE ACTION EQUATION

In order to model radar imagery of the ocean, it is necessary to determine the amplitudes of water waves and their spatial variation. For this purpose, the conservation of wave action is utilized, given by [2]

$$\frac{\partial}{\partial t}\left(\frac{\langle E\rangle}{\omega}\right) + (\mathbf{U} + \mathbf{c}_g)\cdot\nabla\left(\frac{\langle E\rangle}{\omega}\right) + [\nabla\cdot(\mathbf{U} + \mathbf{c}_g)]\left(\frac{\langle E\rangle}{\omega}\right) = 0, \tag{1}$$

where $\langle E\rangle$ is the energy per unit volume of a wave packet centered at x at time t traveling through the water and $\mathbf{U}$ is the surface current. The group velocity vector is

$$\mathbf{c}_g = \frac{\partial\omega}{\partial k_x}\hat{i} + \frac{\partial\omega}{\partial k_y}\hat{j}, \tag{2}$$

where ω is the intrinsic frequency and $k_{x(y)}$ is the component of the wave number along the orthogonal direction specified by $\hat{i}(\hat{j})$. The intrinsic frequency is given by the dispersion relation

$$\omega^2 = \left(gk + \frac{Tk^3}{\rho}\right)\tanh(kD), \tag{3}$$

where g is the acceleration of gravity, ρ is the density of the water, T is the surface tension, and $D = D(x, y)$ is the depth of the water.

For a continuous spectrum, it is convenient to recast the problem of solving Eq. (1) for the wave action of an individual wave packet in terms of the equivalent problem of solving for the wave action spectral density [3], $A(\mathbf{x}, \mathbf{k}, \mathrm{t})$, defined by

$$\frac{\langle E\rangle}{\omega} = A(\mathbf{x}, \mathbf{k}, \mathrm{t})\Delta^2 k, \tag{4}$$

where $\Delta^2 k$ measures the two-dimensional variation (spread) in wave vectors associated with the individual packet. In practise, two procedures have been applied to determine $\langle E\rangle/\omega$, both associated with evaluating A. One of these, referred to as ray tracing, is discussed elsewhere [4]. In this paper, we use the full-wave method, developed by Lyzenga and Bennett [5]. In this case, A is derived from a first-order partial differential equation, with x, y, t, k_x, and k_y as five independent variables and the action spectral density as the only dependent variable.

If one is interested in characterizing the evolution of the action spectral density for a particular surface current feature which is propagating through the ocean with a fixed velocity, the steady-state approximation to the wave-action equation can be employed. The steady-state approximation removes the explicit time-dependence of A by making a Galilean transformation into a reference frame which is fixed upon the feature. The equation to be solved is then

$$(u' + c_{gx})\frac{\partial A}{\partial x} + (v' + c_{gy})\frac{\partial A}{\partial y} - \left(k_x\frac{\partial u}{\partial x} + k_y\frac{\partial v}{\partial x} + \frac{\partial\omega}{\partial x}\right)\frac{\partial A}{\partial k_x} - \left(k_x\frac{\partial u}{\partial y} + k_y\frac{\partial v}{\partial y} + \frac{\partial\omega}{\partial y}\right)\frac{\partial A}{\partial k_y} = S, \tag{5}$$

where S is a general source term which is necessary in order to correctly model ocean waves, which gain energy from the wind and lose energy through a number of dissipation mechanisms, and u' (v') represent the surface current components, u (v) expressed relative to the feature-fixed coordinate system. The computational domain has been reduced to four dimensions with the elimination of time, t, as an independent variable. This is a steady version of the hyperbolic equation, which means that characteristics exist along which a numerical solution can be propagated through the region. In addition, if the source term S is quadratic in A (as in Eq. (7)), when Eq. (5) is expressed in finite difference form, the resulting expression can be reduced to the solution of a quadratic equation. Since the equation is hyperbolic, this quadratic equation can be solved uniquely to provide A, provided it is possible to identify which of the two roots of the equation is the appropriate one. Because the action density is positive definite, this choice can be uniquely specified by identifying situations in which the coefficients of A in the finite difference expression share a common sign.

The action spectral density can alternatively be written as $A(x, y, k, \phi)$, with the wave number magnitude k and angle ϕ defined as

$$k = (k_x^2 + k_y^2)^{1/2}, \quad \phi = \tan^{-1}(k_y/k_x). \tag{6}$$

In the present calculations, the Plant–Hughes form is employed for the source function, defined by [6]

$$-\beta\frac{A}{A_0}(A - A_0), \tag{7}$$

where A_0 is the equilibrium action density given by Bjerkaas and Riedel [7]. Here β is the wave growth-relaxation rate defined by Plant [8],

$$\beta = 0.04 \left(\frac{u_*}{c}\right)^2 \omega |\cos(\phi - \phi_w)|, \tag{8}$$

where u_* is the friction velocity, $c = \omega/k$ is the wave phase velocity, and ϕ_w is the wind direction.

In practice, Eqs. (5)–(8) are solved by writing Eq. (5) in finite difference form, based on an initial set of values defined by the values of A as a function of wave vector, at each point along a particular boundary. In particular, using the values of the current, wind, and dispersion relationship (Eq. (3)) at the boundary, nearest neighbor point values for A are derived. The procedure for accomplishing this involves solving a quadratic equation of the form

$$aA^2(i,j,m,p) + bA(i,j,m,p) + c = 0, \tag{9}$$

where

$$a = \beta/A_0, \tag{10}$$

$$b = \frac{u + c_{gx}}{\Delta x} + \frac{v + c_{gy}}{\Delta y} - \beta - \frac{1}{\Delta(\ln k)} \left(-\cos^2\phi \frac{\partial u}{\partial x} - \cos\phi \sin\phi \left(\frac{\partial v}{\partial x} + \frac{\partial u}{\partial y}\right) - \sin^2\phi \frac{\partial v}{\partial y}\right) - \frac{1}{\Delta\phi}\left(-\cos^2\phi \frac{\partial u}{\partial y} - \cos\phi \sin\phi \left(\frac{\partial v}{\partial y} - \frac{\partial u}{\partial x}\right) + \sin^2\phi \frac{\partial v}{\partial x}\right), \tag{11}$$

and

$$c = -\frac{u + c_{gx}}{\Delta x} A(i \pm 1, j, m, p) - \frac{v + c_{gy}}{\Delta y} A(i, j \pm 1, m, p) + \frac{1}{\Delta(\ln k)} \left(-\cos^2\phi \frac{\partial u}{\partial x} - \cos\phi \sin\phi \left(\frac{\partial v}{\partial x} + \frac{\partial u}{\partial y}\right) - \sin^2\phi \frac{\partial v}{\partial y}\right) A(i, j, m \pm 1, p) + \frac{1}{\Delta\phi} \left(-\cos^2\phi \frac{\partial u}{\partial y} - \cos\phi \sin\phi \left(\frac{\partial v}{\partial y} - \frac{\partial u}{\partial x}\right) + \sin^2\phi \frac{\partial v}{\partial x}\right) A(i, j, m, p \pm 1), \tag{12}$$

where the sign of the increments in i, j, m, and p are taken such that the upwind differencing with respect to x, y, k, and ϕ is preserved. (I.e., the sign in each term to be implemented is the opposite of that of the associated coefficient of A.) Note that the terms involving derivatives of ω have been omitted, as we are considering the deep water case where the depth is much larger than any of the wavelengths considered. A is determined using the well-known solution of the quadratic equation. After values of A are determined at points next to the boundary, these values, in turn, are used to initialize computations for subsequent, interior points. Based on this procedure, values of A at all interior points are determined. As noted above, the wave vector variables k_x and k_y from Eq. (5) are expressed in polar form and the radial k variable is constructed using a logarithmically varying scale.

The full-wave formulation of the wave action equation has several drawbacks for this application. It is rather computationally intensive, even in the steady state approximation, which we adopt here. Since the wave action spectral density is calculated at every point in a four-dimensional space, a high resolution calculation requires a great deal of computer memory. A second difficulty of the steady full-wave method is that the action spectral density at the physical boundaries needs to be specified consistent with the dynamics of the equation. In practice, this has usually required that the currents be constrained asymptotically to approach zero at the boundaries so that A can be prescribed there by its equilibrium value, A_0. This requirement has restricted the range of problems for which the method is useful. When a full-wave, high resolution solution is required (which is the case in the radar imaging problem), it is necessary to perform either a single high resolution calculation extending over the entire spatial domain or nested calculations based on the prescription presented below. Because a single high resolution calculation rapidly may become computationally prohibitive, the nesting procedure may be the only viable option for many applications.

III. NESTING CONCEPT

To circumvent some of these difficulties, a nesting procedure was developed in the present work. An important aspect of the nesting procedure is that it provides a practical way of satisfying the self-consistency requirement that a unique solution be obtained from the boundary conditions that are applied at practical infinity. By practical infinity, we are referring to the boundary of the largest mesh used in the problem. The self-consistency requirement is that the solution obtained from the boundary conditions applied at practical infinity can be used to provide boundary conditions for successively smaller meshes subject to the constraint that at some mesh size the solution at interior spatial locations becomes insensitive to further reduction in mesh size. In particular, once the procedure is initialized, based on some prescribed boundary condition (which need not be the one associated with the equilibrium value of A), the nesting procedure provides a method for obtaining appropriately propagated boundary conditions for new numerical grids possessing finer resolution, which are by construction consistent with the equation. The manner in which propagation of boundary conditions occurs is a func-

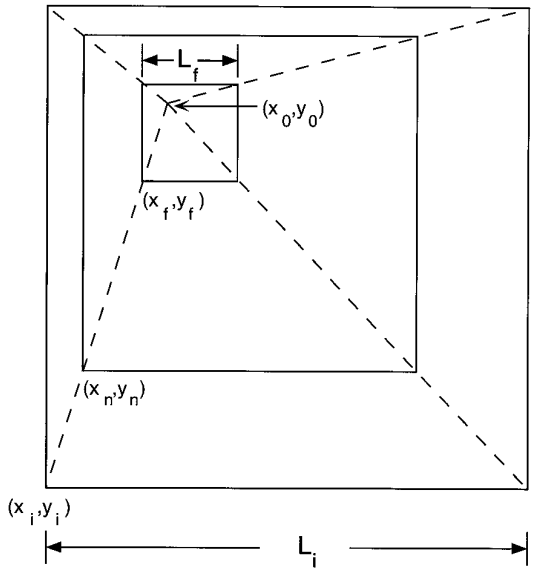

FIG. 1. Drawing illustrating the nesting procedure. $L_{i(f)}$ is the x dimension of the initial (final) grid. The point (x_0, y_0) is the fixed point defined in the text. The points (x_i, y_i), (x_n, y_n) and (x_f, y_f) denote the corners of the initial grid, an intermediate grid and the final grid, respectively.

tion of the growth relaxation time (defined by β^{-1}). When $\beta = 0$, wave action is conserved, so that, for this case, the effects of the boundary condition propagate throughout the entire domain. For finite values of β, a competition exists between the wave transit time and the relaxation time. Thus the boundary effects of longer waves have a larger range of influence. As a consequence, by changing the initial grid size and the initial boundary conditions, it is possible to monitor sensitivities of the spectral dependence of the solution with respect to changes in its boundary values and spatial resolution.

The nested computations are performed in the following manner. The initial region for the calculation is determined by the size of the feature being investigated. The first step is to choose a point of interest, (x_0, y_0), as shown in Fig. 1; this point is referred to as the fixed point. Diagonals are then constructed from (x_0, y_0) to the corners of the original grid. A region of interest, shown by the smallest rectangle in Fig. 1, is then defined; it is dictated by the desired physical final resolution, combined with the chosen numerical size of the spatial grid that results from the constant number of grid points, n_x and n_y, in the x and y directions. The corners of the region of interest are defined by the diagonals. The spatial resolution enhancement, r, is given by the ratio

$$r = L_i/L_f, \tag{13}$$

where $L_{i(f)}$ is the length of the initial (final) region, as shown in Fig. 1. Also, x_n is the position of the lower left corner of the nth stage grid and $x_{i(f)}$ is the position of the lower left corner of the initial (final) stage grid. The remaining parameter to be selected is the number of grids, or stages, M, in the nested calculation.

The nested computation is then carried out as follows. The wave action density is calculated for the initial region. A grid for the next stage is then defined, by a procedure described below, and the wave action density which has been calculated on the initial grid is used to define the boundary condition for the new grid, with the value of the action density being interpolated to the new grid, as necessary. The full-wave method is then applied on this new grid as an initial grid, and the procedure is repeated as often as needed, until the final grid is calculated. As in Lyzenga and Bennett, equilibrium spectral densities are applied at the minimum and maximum wavelength boundaries of the computation. This necessitates that the minimum to maximum wavelength range extend beyond the range of interest for the particular application as discussed in Cooper *et al.* [9].

Once the initial and final grids have been chosen, we can calculate the intermediate grid locations by

$$x_n = x_i + \frac{x_f - x_i}{L_i - L_f}(1 - s^{n-1})L_i, \tag{14}$$

where s is the scale factor, given by

$$s = \left(\frac{L_f}{L_i}\right)^{1/(M-1)} = (r)^{-1/(M-1)}. \tag{15}$$

This divides the total resolution enhancement, r, between the M stages. The y positions are calculated by an analogous equation. The appropriate lengths of the total x dimension of each grid can be calculated simply by scaling the initial x length

$$L_n = s^{n-1}L_i, \tag{16}$$

and the same geometric constraints hold for the y dimension. We note here that the scaling factor must be the same for x as for y. In this procedure, by construction, the relative location of the fixed point in each of the nested grids remains the same. Therefore, if the fixed point is chosen on a mesh point of the initial grid, it remains at the same mesh point of each subsequent, nested grid.

IV. MODELLING OF THE CURRENT FIELD

The motivation for the paper is to demonstrate the utility of a nesting method and to provide preliminary observations based on the method with respect to the variability

and sensitivity of calculated wave spectra as a function of spatial resolution. This work, in turn, has important significance for predictions of large radar returns, such as those observed by Askari [10] near the Gulf Stream during the first High Resolution Remote Sensing Experiment [11]. In particular, the radar image is shown in Fig. 2a. Figure 2b shows the result of applying the composite radar backscatter model to a model (described below) of the underlying currents without the application of nesting to refine the spatial resolution. An important motivation for understanding the role of resolution on radar imagery is provided by the need to understand the marked increase in radar return in the regions of strong curvature (at the points of local maxima and minima) that are present in the sinusoidally displaced feature found in both the measured and simulated images. The surface current distribution that is used to model this rip-like feature is the two-dimensional functional form

$$V(x, y) = -\frac{\delta V}{2}\tanh\left(\frac{x - x_0\sin(2\pi y/\lambda)}{\delta x}\right). \qquad (18)$$

Here, $\delta V = 60$ cm/s is the magnitude of the convergence velocity, $\delta x = 30$ m is the width of the rip, $x_0 = 300$ m is the amplitude of the sinusoidal displacement of the convergence, and $\lambda = 1500$ m is the wave length of the displacement. The magnitudes of δV and δx are representative values, inferred from ground truth measurements by Marmorino and Trump [12], and the values of x_0 and λ were inferred from a section of the radar image (Fig. 2a). (In particular, the sinusoidal form wavelength was inferred from the meandering red line located between 6.5 and 8 km in the azimuthal direction and approximately 1.4 km in the range direction.) A sketch of the overall geometry is shown in Fig. 3a. Figure 3b shows a one-dimensional cut of the current profile at $y = 0$, illustrating the form of the convergence and the magnitude of the parameters used in the modelling.

The choice of currents represented by Eq. (18) is a two-dimensional extension of a similar one-dimensional form used by Jansen *et al.* [13]. This form is derived by sinusoidally displacing the one-dimensional convergence to mimic the shape of a section of the experimental radar image (Fig. 2a), providing a simple two-dimensional variability in the single component current field. This 2D-field possesses a current shear, in addition to the convergence, with the ratio of shear to convergence varying with y. Because an analytic representation is used, interpolation is not necessary, even when currents of arbitrarily fine resolution are constructed.

V. RESULTS

The initial computational domain included for all the nesting computations is a rectangle of dimension 1000 m by 1500 m shown in Fig. 3a. Two areas of interest (final computational domains), both of dimension 200 m by 300 m, constructed through nesting, are shown in Fig. 3a as regions 1 and 2. Region 2 possesses a large ratio of shear to convergence while region 1 has a minimal ratio. We chose a mesh in which the number of points n_x and n_y in the x and y directions, respectively, was given by $n_x = n_y = 61$, so that the beginning resolution was 25×16.6 m and the final resolution was 5×3.3 m, representing a fivefold resolution enhancement ($r = 5$).

In these calculations, the wave vector $\mathbf{k}$ is expressed in polar form, as in Eq. (6), using n_k radial values ($k(l)$, $l = 1, 2,..., n_k$) and n_P azimuthal directions ($\phi(m)$, $m = 1, 2,..., n_p$). It is advantageous to use an exponential scale for the wave vector magnitude since many decades of k variation are typically included. This is accomplished by defining k and ϕ by

$$k(l) = k_{\min}\left(\frac{k_{\max}}{k_{\min}}\right)^{(l-1)/(n_k-1)} \qquad (19)$$

and

$$\phi(m) = \frac{2\pi(m-1)}{n_p}. \qquad (20)$$

Each nesting configuration as defined above provides enhancements in spatial resolution for fixed spectral resolution, defined by n_k, n_p, $k_{\max}$, and $k_{\min}$ in Eqs. (19) and (20).

Two levels of spectral resolution, (n_k, n_p), were utilized in the present work: (32, 30) and (32, 64). In all the computations conducted, $k_{\max} = 6283$ m^{-1} and $k_{\min} = 0.126$ m^{-1}, corresponding to 0.001 m and 50 m for the minimum and maximum wavelengths. The minimum wavelength is selected to be significantly smaller than the wavelength of interest. As discussed in Cooper *et al.* [9], this is because, for the functional form that is assumed in Eq. (5), $\beta \propto k^{1/2}$ and, hence, $A \to A_0$ as $k \to \infty$. The 50-m maximum wavelength is chosen because it is well beyond the peak in the equilibrium spectrum for the 3 m/s winds used in the calculations [5, 9]. Also, the deep water approximation to the dispersion relation was used throughout, so that the hyperbolic tangent term in Eq. (3) was taken as unity. Initial nesting computations were performed using $n_k = 32$ and $n_p = 30$, and $M = 6$ and $M = 11$ for the same resolution enhancement, $r = 5$. These two overlapping values of M were used to enable a direct comparison of the action spectral density at corresponding equal intermediate meshes in the nests, as well as at the common final mesh.

Convergence at a fixed value of M was monitored using the quantity C_M defined by

$$C_M(i) = \frac{F_M(i+1) - F_M(i)}{F_M(i+1) + F_M(i)}, \quad i = 1, M-1, \qquad (21)$$

a

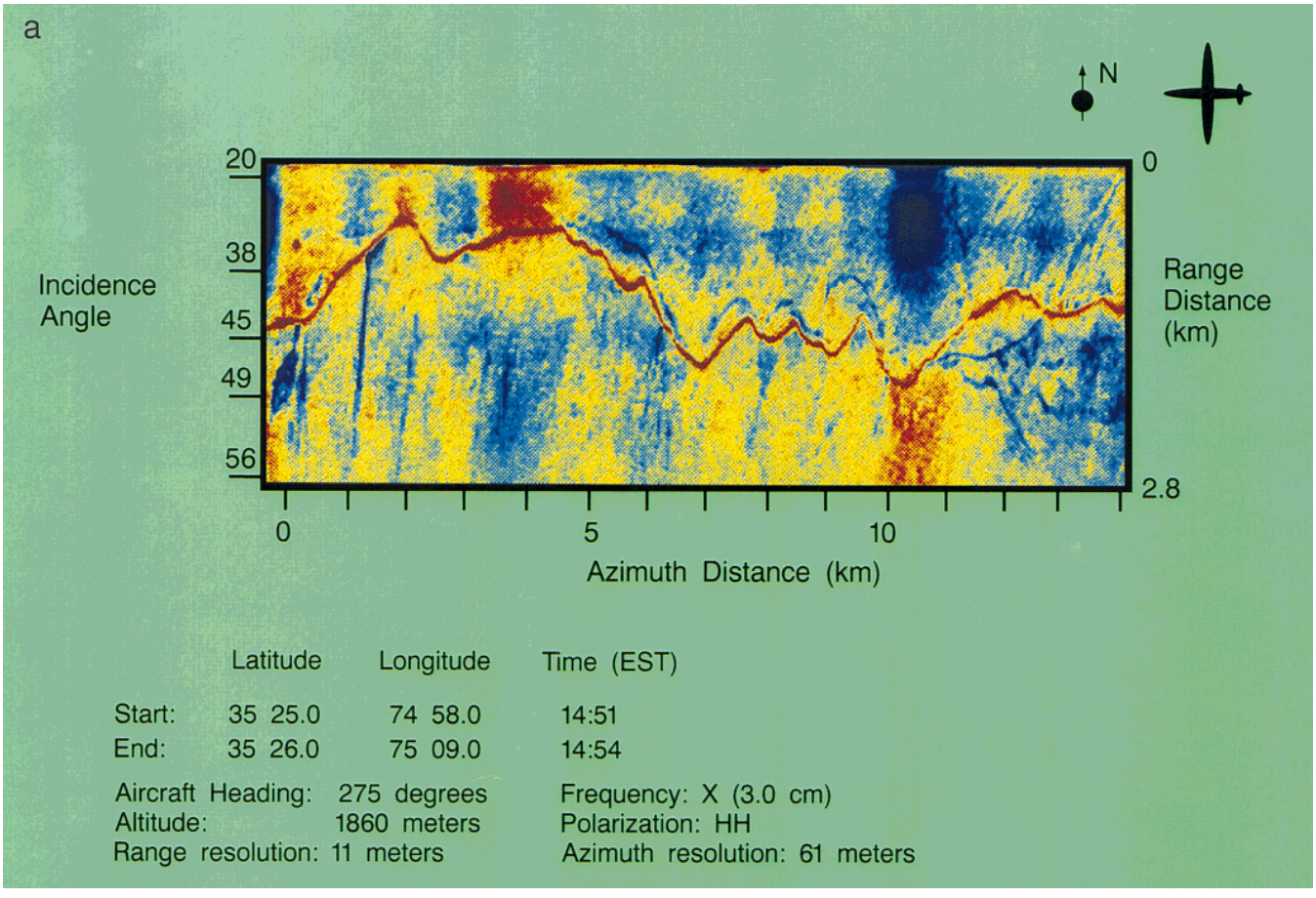

	Latitude	Longitude	Time (EST)
Start:	35 25.0	74 58.0	14:51
End:	35 26.0	75 09.0	14:54

Aircraft Heading: 275 degrees
Altitude: 1860 meters
Range resolution: 11 meters
Frequency: X (3.0 cm)
Polarization: HH
Azimuth resolution: 61 meters

b

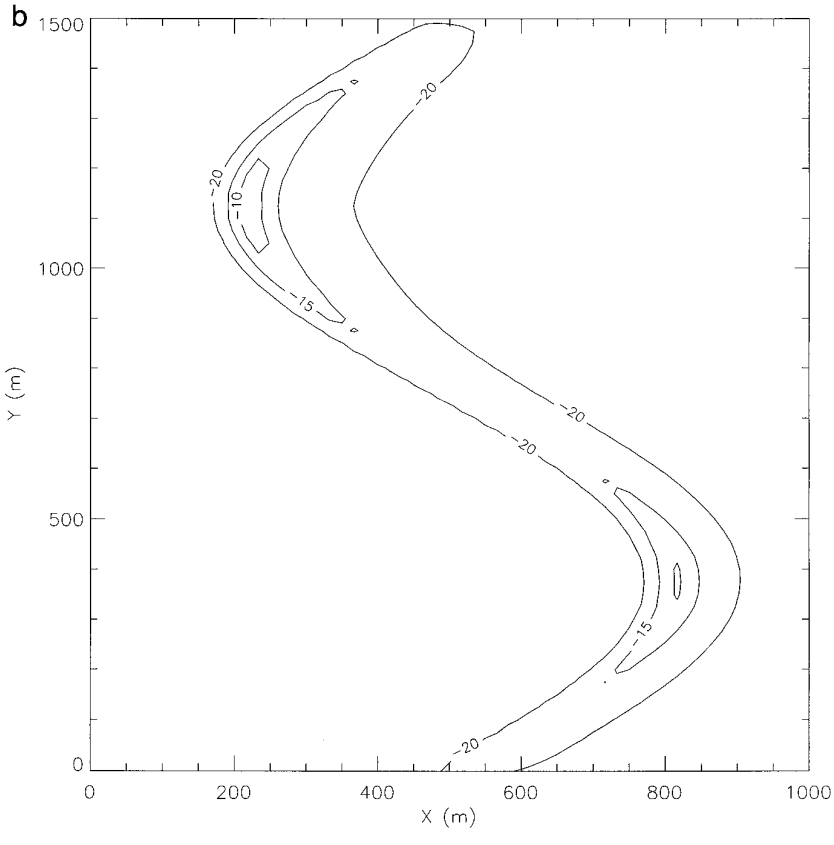

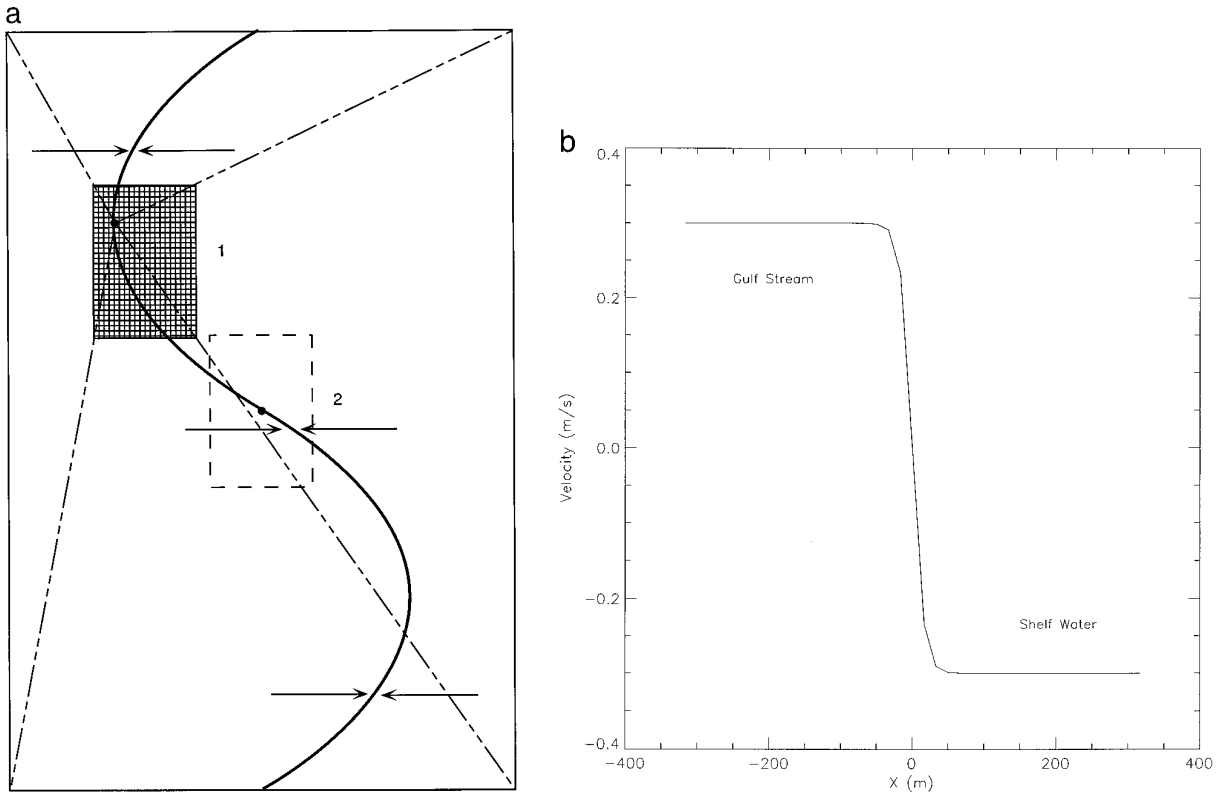

FIG. 3. (a) A drawing of the model of the rip used in these calculations. The two locations of the regions where the nesting procedure was terminated are shown by the small rectangles labeled 1 and 2. The fixed point for each area is shown by the small dot. The arrows show the convergence of the current to the rip, which has been displaced sinusoidally to model the variations seen in Fig. 2. (b) A one-dimensional view of the current convergence, showing the parameters which were used.

where $F_M(i)$ is the wave height spectral density at the fixed point for stage i of M. Here, the wave height spectrum is defined by

$$F = \frac{k}{\omega} A. \tag{22}$$

Convergence of the calculation was determined from contour plots of $C_M(i)$. Two of these plots are shown in Fig. 4, for the case where $(n_k, n_p) = (32, 64)$ and $M = 11$. It is seen that the change in spectral density from one stage of the nest to the next is diminishing as the nesting process evolves. At the final stage (shown in Fig. 4b), except for a small region in the neighborhood of the origin, maximum values of C_M relax to somewhat less than 0.08. Similar convergence behavior was found for $M = 6$ with somewhat larger values for C_M. Convergence of this type was also obtained for $(n_k, n_p) = (32, 30)$.

To investigate the uniqueness of the converged result, we define the fractional spectral density difference D as

$$D = \frac{F_6(i) - F_{11}(j)}{F_6(i) + F_{11}(j)}, \tag{23}$$

where $F_6(i)$ (as in Eq. (22)) is the wave height spectral density at the fixed point for the ith stage of $M = 6$ and $F_{11}(j)$ is the wave height spectral density at the equivalent stage j of $M = 11$. The first stage is based on the case in which the equilibrium values A_0 are used for the boundary conditions. The computational domain and grid that occur

FIG. 2. (a) An X-band, horizontally polarized, real aperture radar image of the rip, taken during the first High Resolution Remote Sensing experiment, showing the variation in radar cross section in decibels. The intensities vary from about 15 db below the background level (dark blue) to about 10 db above (red). The sinusoidally displaced red line running horizontally through the image corresponds well with the location of a current convergence seen in ground truth measurements. (b) Contour plot of the model radar cross section per unit area, expressed in decibels, calculated using the composite scattering model. Because the absolute magnitude of the cross section is used, all values are negative. The underlying hydrodynamics are calculated by the full-wave method, with $n_k = 32$ and $n_p = 64$.

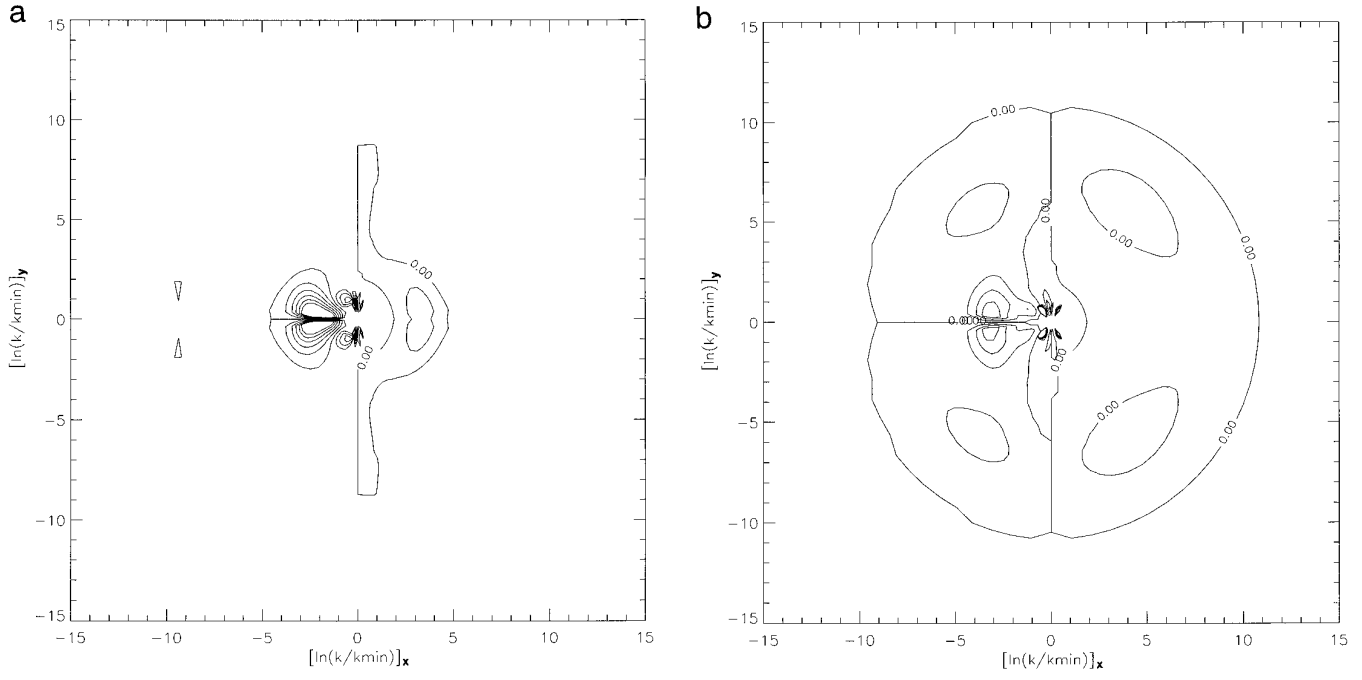

FIG. 4. Contour plots of the convergence parameter $C_M(i) = (F_M(i+1) - F_M(i))/(F_M(i+1) + F_M(i))$ for $i = 1$ (a) and 10 (b). Contours are incremented in steps of 0.02. The convergence of the calculation is seen in the increase in area of the zero contour and the decrease in area of the $C_M = 0.1$ contour, which is the largest value shown. The ordinate and abscissa are the y and x components of $\ln(k/k_{\min})$. The origin therefore represents k = $k_{\min}$ or $\lambda = 50$ m while the outer extremes of the figure represent $\ln(k/k_{\min}) = 10.819$ or $\lambda = 0.001$ m.

at stage 3 for $M = 11$ are exactly the same as the grid and domain that are present at stage 2 for $M = 6$. Similarly, equivalent grids are obtained for the jth stage for $M = 11$ and the ith stage for $M = 6$, when $j = 2i - 1$. The maximum and minimum values for D (measured at the fixed point) for each set of equivalent stages are shown in Table I.

As discussed above, for $(n_k, n_p) = (32, 30)$, the nesting procedure seems to converge to a particular solution as mesh size is reduced. However, the resulting solution is not correct. This failure can be seen by comparing equivalent calculations (such as $M = 6$ and $M = 11$) using Eq. (23). In particular, in Table I, in the column labeled $n_p = 30$,

TABLE I

The Maximum and Minimum of the Fractional Difference D, Defined by Eq. (23), of the Wave Height Spectral Density for Equivalent Grids for Calculations with $M = 6$ and $M = 11$ for three sets of parameters

Stage of $M = 6$	Stage of $M = 11$	$n_p = 64$, $n_k = 32$, Region 2		$n_p = 64$, $n_k = 32$, Region 1		$n_p = 30$, $n_k = 32$, Region 1	
		Max	Min	Max	Min	Max	Min
2	3	0.0019	−0.0007	0.0005	−0.0014	1.0000	−1.0000
3	5	0.0036	−0.0009	0.0007	−0.0105	1.0000	−1.0000
4	7	0.0091	−0.0028	0.0015	−0.0259	1.0000	−1.0000
5	9	0.0058	−0.0051	0.0031	−0.0236	1.0000	−1.0000
6	11	0.0034	−0.0139	0.0053	−0.0234	1.0000	−1.0000

Note. The stages that are used in computing D are listed in the first two columns. Regions 1 and 2 refer to the rectangles labeled 1 and 2, respectively, of Fig. 3a. The small differences for both of the cases with $n_p = 64$ show that convergence to a unique solution with respect to the number of nesting stages has been reached by $M = 6$ and $M = 11$, in contrast to the $n_p = 30$ case, where convergence to a unique solution has not been achieved.

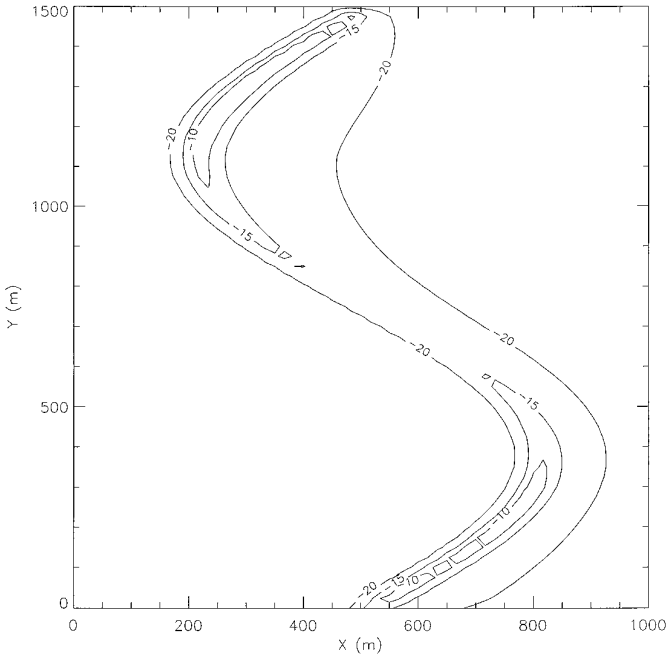

FIG. 5. Contour plot of the model radar cross section in decibels, calculated using the composite scattering model. The underlying hydrodynamics are calculated by the full-wave method, with $n_k = 32$ and $n_p = 30$.

the minimum and maximum values of D are always plus or minus one (to the numerical accuracy displayed), which shows that at the fixed point, for at least one set of spectral (k, ϕ) values, the two calculations differ by many orders of magnitude. As a consequence, the solution for $(n_k, n_p) = (32, 30)$ is, at each equivalent stage, very different, and the procedure, when applied with $n_p = 30$, has failed to provide a solution that asymptotically (as a function of spatial mesh size) approaches the correct (''unique'') result. A condition for obtaining a unique solution is that the two calculations provide approximately the same result for all spectral values, which gives $|D| \ll 1$.) We found similar results in comparing calculations with $M = 21$ and $M = 11$ for $n_p = 30$.

However, as can be seen by the marked reduction in the values for $|D|$ in the table, when n_p is increased from 30 to 64 with n_k kept fixed at 32, $(n_k, n_p) = (32, 64)$, values of $|D|$ are significantly reduced at the fixed point. In particular, the two columns in Table I labeled $n_p = 64$ show that the maximum values of $|D|$ (which increase, but not significantly, as the procedure progresses) for the areas labeled 1 and 2 of Fig. 3a are all below 0.026. The small sizes of these values indicate stability with respect to the iteration procedure and show that the calculation with $M = 6$ has converged to a solution closely approaching the solution for $M = 11$, strongly suggesting that the nesting result is unique.

Calculations of the radar backscatter cross section also show a sensitivity to the n_p value. Figure 5 shows the result of an RCS calculation, based on the $n_p = 30$ spectral density results. The skewed shape of the interior contours contrasts with the more symmetric shape of the corresponding contours in Fig. 2b. The origin of this asymmetry was identified from a comparison of the spectral densities for the two cases and was found to be primarily due to waves with a wavelength of about four meters. These waves are more accurately represented for the case (shown in Fig. 2b) in which $n_p = 64$.

However, this asymmetry was only obtained for the cases involving $(n_k, n_p) = (32, 30)$, when a refined composite backscatter RCS was used. The refinement involves computing the composite backscatter RCS from a complete tilt modulation calculation, in which the procedure for averaging the slopes (S_x, S_y) of individual Bragg scatterers is unconstrained (so that S_x and S_y are allowed to become large). When the more commonly applied small slope approximation [14] is used, the asymmetry is not present. The asymmetry was obtained for all the nested computations at (32, 30) when the complete tilt modulation composite backscatter RCS was employed.

The radar calculation at X-band is not significantly affected by the nesting procedure. However, as indicated above, it is sensitive to the selected spectral resolution parameter (n_p). These sensitivities result from the tilt modulation calculation. Because large slopes are not included in the small slope approximation, the associated tilt modulation calculations are not sufficiently accurate at X-band. When the complete tilt modulation calculation (using all values of the slope) is used, the resulting radar simulation is more sensitive to angular resolution. Thus, a converged radar result is obtained only when the resolution is sufficiently fine.

It is informative to identify the spectral locations where the spectral differences, D, are greatest. To determine this, we examined the wave height spectra as a function of wave number for a given nesting computation. Figure 6 shows the percentage difference in the wave height spectra between the first and last stages for $M = 6$, i.e., between the final nested and the unnested computations. We see that the change in wave height spectra in the range $k = 2$–$10\ \mathrm{m}^{-1}$ is significant, indicating the effect of the nesting procedure is most dramatic for this range of wave vectors. Figure 7 shows the percentage difference between the wave height spectra for the two spectral resolutions $(n_k, n_p) = (32, 30)$ and $(32, 64)$ for the last stage of $M = 6$. The location of the large difference at intermediate wave numbers is a result of the inadequacy of the calculations with $n_p = 30$. Identical plots to those shown in Figs. 6 and 7 occur in the comparable fractional differences in the slope spectra, the curvature spectra and other spectrally resolved moments of F, since the percentage change is the same in F as for its spectrally resolved moments at a particular wave vector.

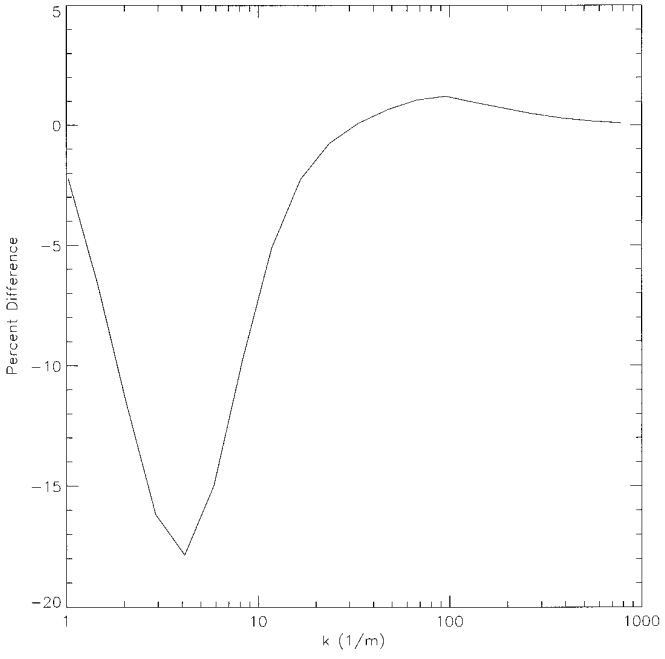

FIG. 6. Plot of the difference of the wave height spectra $D = (F_6(1) - F_6(6))/(F_6(1) + F_6(6))$ for $\phi = 0$, between the first and last stages of a six-stage calculation, as a function of wave number for $(n_k, n_p) = (32, 64)$.

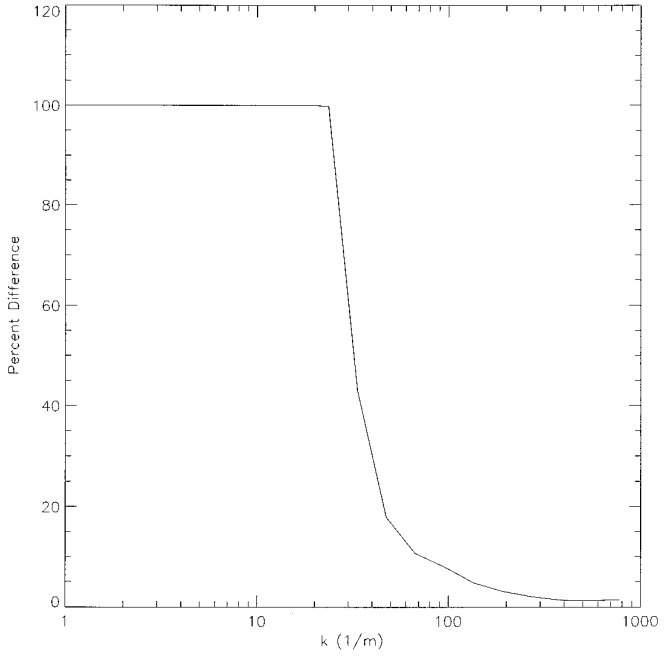

FIG. 7. Plot of the difference of the wave height spectra $D = (F(n_p = 64) - F(n_p = 30))/(F(n_p = 64) + F(n_p = 30))$ from a calculation with $n_p = 30$ compared to one with $n_p = 64$ as a function of wave number. The spectra in both cases are from the last stage of a six-stage calculation.

Having demonstrated unique convergence of the calculation for $M = 6$ and $(n_k, n_p) = (32, 64)$, we attempted to determine the minimum number of stages required for convergence. Somewhat surprisingly, it was found that convergence is satisfactory for $M = 2$, although the values of D and C_M are somewhat higher when comparing $M = 2$ with $M = 6$, than for the comparison of $M = 6$ with $M = 11$. However, it is worthwhile noting that this rapid convergence with respect to the application of the nesting procedure is only valid when n_p is sufficiently large. (As shown above, when $n_p = 30$, A converges to an incorrect limit when the nesting procedure is applied.) Convergence for $M = 2$ at $(n_k, n_p) = (32, 64)$ seems to indicate that the computation of the wave action spectral density is more sensitive to changes in the resolution of the spectral parameters than to variations in the scale associated with the spatial resolution. Investigations at intermediate spectral resolutions, may be useful to exploit this behavior. A procedure involving simultaneous nesting in the spectral domain may also be beneficial.

VI. SUMMARY

A technique has been developed which extends the effectiveness of time independent, full wave techniques for solving the wave action equation, such as the one used in the full-wave method of Lyzenga and Bennett. The value of the procedure comes from its usefulness for identifying a solution that asymptotically approaches the unique solution which would occur in the limit of small spatial and spectral resolution. A requirement for identifying such a solution is that the solution be insensitive with respect to further changes in spatial and spectral resolution. Because the procedure provides a method for altering the spatial resolution and updating the boundary condition values that are used to initiate the calculation, the method provides a technique for rapidly changing the spatial resolution and determining whether a converged result can be obtained with respect to this form of variation. Because this form of variation can be implemented rapidly as a result of the procedure, it is also possible to investigate the effects of changing the spectral resolution. We have demonstrated this in tests.

The technique utilizes wave action spectral densities calculated on an exterior grid to define appropriate boundary conditions for a calculation on a smaller, interior grid with higher spatial resolution. Since this procedure could, in principle, be used recursively, it is referred to as nesting. In tests of this techique, it is found that, with sufficiently fine spectral resolution, one nesting step was sufficient to guarantee unique convergence. In the process, we have identified a number of sensitivities associated with the choice of wave vector resolution that have bearing on the problem of determining correct spectra on successively more finely resolved spatial grids.

From these results, it is concluded that the choice of angular resolution in spectral space, which was initially deficient, can more significantly alter the result than the choice of spatial resolution scale. It is suggested that an optimal choice of wave number parameters may occur intermediate between the two choices used in these calculations, and that for this choice, changes in spatial scale resolution may affect the results more dramatically. It should also be possible to perform a spectral nesting procedure through which more finely resolved spectral parameters are obtained simultaneously with more finely resolved spatial resolution.

In order to obtain a unique solution, with respect to variations in resolution (both spatial and spectral), there are two problems that are inherent in the method: 1. Errors may result in portions of the spectrum through the propagation of boundary condition effects; 2. Because a first-order discretization algorithm is being applied, at any stage during a series of nested calculations, uncontrolled numerical errors may arise. In the present paper, we have examined the sensitivities associated with the application of the first-order algorithms as they relate to variations in spatial resolution. In particular, we have performed computations with two nested grids where we have demonstrated that the results are internally consistent with the requirement that when calculations are performed with identical resolution, errors are insignificant. This test does not preclude the possibility that the unique solution has not been obtained. To more conclusively identify the uniqueness of the solution, it would be desirable to construct a single, highly resolved solution at the finest resolution. However, because of the large computational requirements for such a calculation, these computations have not yet been performed for the present feature. Also, although we have determined that the solution is relatively insensitive to the effects of changes in the boundary condition at the coarsest resolution, we have not extensively examined the effects of boundary condition propagation at the finest resolution. In a future paper, we will conduct a more detailed series of computations to optimize the procedure and provide a detailed comparison of our results with relevant experiments.

ACKNOWLEDGMENTS

The authors thank Drs. John Bennett and Gaspar Valenzuela for helpful discussions concerning applications of the nesting procedure and the full-wave model. This work was supported in part by a grant of HPC time from the DoD HPC Center, CEWES Cray C90. Work supported by the joint Naval Research Laboratory/Office of Naval Research Accelerated Initiatives, High Resolution Remote Sensing and Physics of Coastal Remote Sensing.

REFERENCES

1. E. Attema, "The ERS-1 Geophysical Validation Program for Wind and Wave Data Products," in *Proceedings, Workshop on ERS-1 Geophysical Validation, Penhors, France, April 27–30, 1992,* p. 1–3.
2. F. P. Bretherton and C. J. R. Garrett, *Proc. R. Soc. London, Ser. A* **302,** 211 (1969).
3. O. M. Phillips, *The Dynamics of the Upper Ocean,* 2nd ed. (Cambridge Univ. Press, New York, 1977).
4. P. H. LeBlond and L. A. Mysak, *Waves in the Ocean* (Elsevier, New York, 1978), p. 23.
5. D. R. Lyzenga and J. R. Bennett, *J. Geophys. Res. C* **10,** 12345 (1988).
6. B. A. Hughes, *J. Geophys. Res.* **83,** 455 (1978).
7. A. W. Bjerkaas and F. W. Riedel, Rep. TG-1328, Appl. Phys. Lab., Johns Hopkins University, 1979 (unpublished).
8. W. J. Plant, *J. Geophys. Res.* **87,** 1961 (1982).
9. A. L. Cooper, S. R. Chubb, F. Askari, G. R. Valenzuela, J. R. Bennett, and W. C. Keller, *J. Geophys. Res.* **99, C4,** 7865 (1994).
10. F. Askari, Multitemporal analysis of radar imagery for study of a cuspate convergent front on the continental shelf, *J. Geophys. Res.* submitted.
11. R. P. Mied, F. Askari, G. O. Marmorino, G. R. Valenzuela, and D. B. Trizna, "High Resolution Remote Sensing," in *1992 NRL Review,* edited by J. D. Bultman (Naval Research Laboratory, Washington, DC, 1992), p. 181.
12. G. O. Marmorino and C. L. Trump, *J. Geophys. Res.* **99, C4,** 7627 (1994).
13. R. W. Jansen, T. L. Ainsworth, R. A. Fusina, S. R. Chubb, and G. R. Valenzuela, *International Geoscience and Remote Sensing Symposium Digest* (1994), p. 460.
14. J. W. Wright, *IEEE Trans. Antennas Propag.* **AP-16,** 217 (1968).